International Journal of Nanomedicine

Dovepress

open access to scientific and medical research

Open Access Full Text Article

ORIGINAL RESEARCH

Nanoformulation of the Broad-Spectrum Hydrophobic Antiviral Vacuolar ATPase Inhibitor Diphyllin in Human Recombinant *H*-ferritin

Michaela Vojnikova[1,2,*], Martina Sukupova[1,3,*], Michal Stefanik[1,4], Petra Strakova[3–5], Jan Haviernik[4], Katerina Kapolkova[1], Eliska Gruberova[1], Klara Raskova[1], Hana Michalkova[1], Pavel Svec[1], Marie Peskova Kudlickova[1], Ivana Huvarova[4], Daniel Ruzek[3–5], Jiri Salat[3–5], Vladimir Pekarik[1], Ludek Eyer[3–5], Zbynek Heger[1]

[1]Department of Chemistry and Biochemistry, Mendel University in Brno, Brno, Czech Republic; [2]Central European Institute of Technology, Brno University of Technology, Brno, Czech Republic; [3]Department of Experimental Biology, Faculty of Science, Masaryk University, Brno, Czech Republic; [4]Department of infectious Diseases and Preventive Medicine, Veterinary Research Institute, Brno, Czech Republic; [5]Institute of Parasitology, Biology Centre of the Czech Academy of Sciences, Ceske Budejovice, Czech Republic

*These authors contributed equally to this work

Correspondence: Zbynek Heger, Research Group for Molecular Biology and Nanomedicine, Department of Chemistry and Biochemistry, Mendel University in Brno, Brno, CZ-613 00, Czech Republic, Tel +420-5-4513-3350, Fax +420-5-4521-2044, Email heger@mendelu.cz

Background: As highlighted by recent pandemic outbreaks, antiviral drugs are crucial resources in the global battle against viral diseases. Unfortunately, most antiviral drugs are characterized by a plethora of side effects and low efficiency/poor bioavailability owing to their insolubility. This also applies to the arylnaphthalide lignin family member, diphyllin (Diph). Diph acts as a vacuolar ATPase inhibitor and has been previously identified as a promising candidate with broad-spectrum antiviral activity. However, its physicochemical properties preclude its efficient administration in vivo, complicating preclinical testing.

Methods: We produced human recombinant *H*- ferritin (HsaFtH) and used it as a delivery vehicle for Diph encapsulation through pH-mediated reversible reassembly of HsaFtH. Diph nanoformulation was subsequently thoroughly characterized and tested for its non-target cytotoxicity and antiviral efficiency using a panel of pathogenic viral strain.

Results: We revealed that loading into HsaFtH decreased the undesired cytotoxicity of Diph in mammalian host cells. We also confirmed that encapsulated Diph exhibited slightly lower antiviral activity than free Diph, which may be due to the differential uptake mechanism and kinetics of free Diph and Diph@HsaFtH. Furthermore, we confirmed that the antiviral effect was mediated solely by Diph with no contribution from HsaFtH.

Conclusion: It was confirmed that HsaFtH is a suitable vehicle that allows easy loading of Diph and production of highly homogeneous nanoparticles dispersion with promising broad-spectrum antiviral activity.

Keywords: drug delivery, SARS-CoV-2, TBEV, WNV, Zika virus

Introduction

Globalization, global climate change, and our way of life all increase the possibility of viral epidemics or pandemic outbreaks, such as the Spanish flu in 1918–1919, Zika in 2015–2016, and more recently the COVID-19 pandemic, which is estimated to have caused more than 6.7 million deaths.[1] Despite this, the development of efficient broad-spectrum antiviral agents remains a major challenge for the scientific community.

Currently, no broad-spectrum antivirals are available; however, a plethora of antiviral drugs is routinely used to treat a variety of viral infections. Among them, remdesivir, oseltamivir, zalcitabine, ritonavir, acyclovir and others might be mentioned.[2] Unfortunately, it should be noted that these drugs are frequently characterized by poor bioavailability, low solubility, poor permeability, short half-life, and side effects that hinder their efficient utilization.[3] Therefore, stimulated

Received: 28 November 2023
Accepted: 8 April 2024
Published: 30 April 2024

by worldwide needs due to the ongoing COVID-19 pandemic, a plethora of de novo synthesized compounds or compounds isolated from various natural sources have been tested as potential novel antiviral compounds.

Among them, diphyllin (Diph), a natural compound of the arylnaphthalide lignin family, seems to be a promising broad-spectrum antiviral candidate.[4,5] Diph [1-hydroxy-2-(hydroxymethyl)-6,7-dimethoxy-4-(3,4-methylenedioxy-phenol)-3-naphthoic acid-γ-lactone] and its derivatives have initially been shown to inhibit V-ATPase activity in human osteoclasts.[6] V-ATPases are proton pumps that acidify the endosomal lumen.[7] It is noteworthy that acidic endosomal pH is a crucial prerequisite for fusion of the viral envelope with the endosomal membrane;[8] therefore, blocking acidification of endosomes through inhibition of V-ATPases appears to be a promising broad-spectrum antiviral strategy. Unfortunately, Diph and its derivatives have poor solubility, and thus exhibit poor bioavailability in vivo. Therefore, approaches to improve the solubility and bioavailability of Diph while retaining or enhancing its antiviral activity are of utmost importance.

One possible solution is the formulation of Diph into nanoscaled particles. These have been shown to improve bioavailability and enhance drug exposure for a wide spectrum of administration scenarios.[9] To the best of our knowledge, Diph has been successfully loaded only into polymeric nanoparticles composed of poly(ethylene glycol)-block-poly(lactide-co-glycolide) (PEG-PLGA). Subsequently, the functionality of these nanoparticles has been validated in H1N1 influenza[10] and type II feline infectious peritonitis viruses.[11]

In the present study, we used another type of organic nanoparticles formed by recombinant human *H*-ferritin (HsaFtH). In contrast to polymeric nanoparticles, protein-based nanomaterials are highly homogeneous, biodegradable, and biocompatible. Ferritin-based nanoformulations are susceptible to digestion in the gastrointestinal tract. Thus, they are mostly intended for intravenous administration, after which they are able to circulate in the bloodstream. Furthermore, due to the inherently high expression of TfR1 on blood-brain barrier; *H*-rich ferritins can even be transcytosed to the brain.[12] Due to their protein nature, ferritins can be produced using recombinant technologies and no other complicated manufacturing technologies are needed.[13] Ferritins are ubiquitously expressed proteins capable of storing iron, thus protecting cells against free radicals generated in the Fenton reaction,[14] and are well known for their ability to reversibly self-assemble their symmetrical spherical architecture in acidic environments. This phenomenon can be exploited to encapsulate a variety of bioactive molecules into the inner cavity with an 8-nm diameter.[15–18] Although the specific mechanisms of release of low mass payloads from the inner cavity are not yet fully understood, it has been suggested that drugs are gradually released due to acidification of the endolysosomal compartments,[19] and also plausibly due to the proteolytic activity of endolysosomal enzymes.[20] This property makes ferritins highly promising pH-responsive nanovehicles suitable for the delivery of V-ATPase inhibitors; since after endocytosis and acidification of endosomes, ferritins gradually release inhibitors, which block the fusion between the viral envelope and endosomal membrane, thus inhibiting subsequent viral escape to the cytoplasm (depicted in Scheme 1).

Considering the advantageous properties of ferritins, the objective of this study was to optimize the first nanoformulation of Diph, not based on synthetic polymers, and to determine the ability of Diph encapsulated in recombinant human *H*-ferritin (HsaFtH) to inhibit various types of viruses [Zika virus (ZIKV), West Nile virus (WNV), tick-borne encephalitis virus (TBEV), and severe acute respiratory syndrome-related coronavirus (SARS-CoV-2)].

Materials and Methods

Chemicals

Chemicals were purchased from Sigma-Aldrich (St. Louis, MO, USA) unless otherwise noted. Diph was synthesized by Apigenex (Prague, Czech Republic).

Production and Characterization of Recombinant Human HsaFtH

Recombinant HsaFtH was produced using BL21-CodonPlus (DE3)-RIL *E. coli* (Agilent, Santa Clara, CA, USA).[21] Bacteria were incubated overnight at 37 °C in LB medium (10 g/L bacto-tryptone, 10 g/L NaCl, and 5 g/L yeast extract) supplemented with kanamycin and chloramphenicol (50 µg/mL and 34 µg/mL, respectively). The bacteria were harvested by centrifugation and inoculated into fresh LB medium (w/ 50 µg/mL kanamycin and 34 µg/mL chloramphenicol). After 1 h of incubation, the bacteria were induced with 0.5 mM isopropyl β-D1-thiogalactopyranoside and cultured for 4 h. The bacteria were then collected by centrifugation and resuspended in ferritin lysis buffer (FLB; 25 mM ½ Na HEPES, 150 mM NaCl). Bacteria were

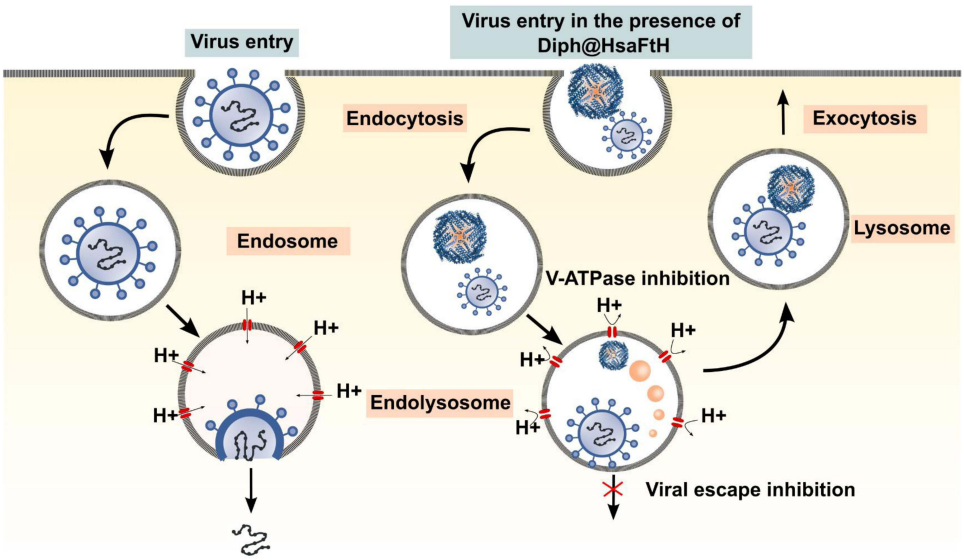

Scheme 1 Depiction of entry and endosomal escape of an enveloped virus with or without the presence of Diph@HsaFtH.
Abbreviations: Diph, diphyllin; HsaFtH, human *H*-ferritin.

disintegrated by sonication with a Q700 sonicator (QSonica, Newtown, CT, USA), centrifuged, and the cleared lysate was transferred to a new tube. Mesophilic proteins were denatured by heating for 10 min at 70 °C. The lysate was cooled on ice, and denatured proteins were removed by centrifugation. The clear supernatant was transferred to a new tube and treated with DNase I (10 µg/mL) at 37 °C overnight to remove bacterial DNA. DNase I and residual proteins were removed from the sample by a second heat denaturation at 85 °C for 10 min, followed by cooling and centrifugation. Following $(NH_4)_2SO_4$ precipitation was done in two steps. First, a suboptimal amount of $(NH_4)_2SO_4$ was used to precipitate unwanted proteins that were removed by centrifugation. The cleared supernatant was mixed with a final concentration of $(NH_4)_2SO_4$ (400 mg/mL) to precipitate HsaFtH. The precipitate was collected by centrifugation. The isolated protein precipitate was washed three times with ammonium sulfate (400 mg/mL in water), dissolved in FLB, and desalted using size-exclusion chromatography (SEC) on PD MiniTrap G-25 Sephadex columns (GE Healthcare, Wauwatosa, WI, USA). Protein concentration was quantified using the Bradford assay (Bio-Rad, Hercules, CA, USA). The morphology and size distribution of recombinant HsaFtH were examined by transmission electron microscopy (TEM, Tecnai F20, FEI, Eindhoven, The Netherlands) and dynamic light scattering (DLS, Zeta Sizer Nano, Malvern Instruments, Malvern, UK), according to our previously published study.[22]

Preparation and Characterization of Diph@HsaFtH

Diph was dissolved in dimethyl sulfoxide (DMSO) at 5 mg/mL and diluted with Na_2HPO_4-NaH_2PO_4 (200 mM, pH 7) to 1 mg/mL. For encapsulation, HsaFtH was dissociated by adding 1.25 µL of 1 M HCl (pH 4) to 120 µL of 4.3 mg/mL HsaFtH, with subsequent incubation for 15 min at 20 °C. Then, 200 µL of Diph in pH 7.0 buffer was added, and the mixture was incubated for 15 min at 20 °C to induce reassembly of the HsaFtH quaternary structure and to physically entrap Diph in the HsaFtH cavity. To remove the residual unbound Diph, HsaFtH was diafiltrated using Amicon Ultra 50 K (Sigma-Aldrich) with 3× buffer exchange at 6000×g for 15 min. The concentration of encapsulated Diph was quantified via its absorption at 365 nm using a multimode Infinite 200 PRO microplate reader (Tecan, Männedorf, Switzerland). The hydrodynamic diameter (HDD) and polydispersity index (PdI) of Diph@HsaFtH were determined by DLS using a Zetasizer Nano ZS (Malvern Instruments). For this purpose, Diph@HsaFtH was diluted 100× with distilled water, placed in polystyrene cells, and measured at a detector angle of 173°, wavelength of 633 nm, and a temperature of 25 °C, with the refractive index of the dispersed phase 1.45 and 1.333 for a dispersive environment. The same approach was employed to analyze the stability of Diph@HsaFtH at 4 °C and 25 °C. The surface ζ-potential of Diph@HsaFtH diluted 50× with distilled water was analyzed using a Zetasizer Nano ZS (Malvern Instruments). The number of runs varied between 20 and 40, and the calculations considered the diminution of particle concentration based on the Smoluchowski model, with an F(ka) of 1.5 and an equilibration time of 120 s. Morphology

was investigated by TEM with negative staining using Nano-W (Nanoprobes, NY, USA). 4 µL of each sample were deposited onto 400-mesh copper grids coated with a continuous carbon layer. The dried grids were imaged using a Tecnai F20 microscope (FEI). Successful reassociation of Diph@HsaFtH was also validated using 6% native polyacrylamide gel electrophoresis (PAGE) (200 V, 4 °C, 25 min) with NativeMark Unstained Protein Standard, subsequent Coomassie Brilliant Blue staining. Diph@HsaFtH was also analyzed using fast protein liquid chromatography - size-exclusion chromatography (FPLC-SEC) on the Superose 6 Increase 10/300 GL column using the BioLogic DuoFlow System (Bio-Rad, Hercules, CA, USA). The sample was injected using a 500 µL injection loop and eluted isocratically using phosphate-buffered saline (PBS, 0.5 mL/min, room temperature). Detection was performed at a wavelength of 280 nm.

Prediction of Biological Behavior of Diph@HsaFtH

The cumulative release of Diph from Diph@HsaFtH was evaluated after dispersion in Ringer´s solution (pH 7.4) or acidic buffer mimicking the endosomal environment (0.142 g of disodium phosphate, 6.650 g of sodium chloride, 0.071 g of sodium sulfate, 0.029 g of calcium chloride dihydrate, 0.45 g of glycine and 4.1 g of potassium hydrogen phthalate in 1 L of water, pH 5.0) and incubation at 37 °C. At predetermined time points (0, 2, 4, 6, 12, and 24 h), 100 µL aliquots were collected after centrifugation, and the absorption spectra of the released Diph were recorded using Infinite 200 Pro (Tecan). The formation of protein corona was examined after mixing samples with 50% human plasma and separation of surface bound proteins after elution using sodium dodecyl sulfate-gel electrophoresis (SDS-PAGE) as described in our previously published study.[22] To analyze the interactions between human red blood cells (RBCs) and Diph@HsaFtH, RBCs (Fisher Scientific, Waltham, MA, USA) were fixed in 1% glutaraldehyde (30 min, room temperature) and washed with phosphate-buffered saline (pH 7.4). The RBCs were then centrifuged (200×*g*, 10 min) and dehydrated using a series of ethanol solutions (40–90%, 5 min, 100%, 10 min). The RBCs were then fixed using hexamethyldisilazane (30 min) and observed under a MAIA3 scanning electron microscope (SEM) (Tescan, Brno, Czech Republic) equipped with a field-emission gun.

Viral Models and Cell Cultures

Antiviral studies of Diph@HsaFtH were carried out using representatives of the following virus families: (*i*) *Flaviviridae* (WNV, strains 13–104 and Eg-101, and TBEV, strain Hypr, all provided by the Collection of Arboviruses, Institute of Parasitology, Biology Centre of the Czech Academy of Sciences, Ceske Budejovice, Czech Republic), ZIKV, the Brazilian strain Paraiba_01, kindly provided by prof. Paolo M. de A. Zanotto (University of Sao Paolo, Brazil) and ZIKV, strain MR-766 (a representative of the African ZIKV lineage isolated in 1947 in Uganda provided by the European Virus Archive, Marseille, France), and (*ii*) *Coronaviridae* (SARS-CoV-2, strain SARS-CoV-2/human/Czech Republic/951/2020 kindly provided by Dr. Jan Weber from Institute of Organic Chemistry and Biochemistry, Prague, Czech Republic). In all experiments, 0.1 multiplicity of infection (MOI) of the viruses was used for experimental infections. UKF-NB-4, Caco-2, and Vero cells were used for the cell studies. UKF-NB-4 cells (kindly provided by Prof. T. Eckschlager, Motol University Hospital, Prague, Czech Republic) were cultured in IMDM supplemented with 10% fetal bovine serum (FBS), 1% L-glutamine, 100 U/mL penicillin, and 100 µg/mL streptomycin. Caco-2 and Vero cells (ATCC, Manassas, VA, USA) were cultured in DMEM supplemented with 20% (Caco-2) or 10% (Vero) FBS, 1% L-glutamine, 100 U/mL penicillin, and 100 µg/mL streptomycin. Cells were cultured at 37 °C in a 5% CO_2 atmosphere. For all experiments, ~30,000 cells per well in a multi-well plate were added and cultured for 24 h to create a homogeneous monolayer. The use of viral strains and cell lines was approved by institutional review boards of Veterinary Research Institute and Mendel University in Brno.

Evaluation of Cytotoxicity of Diph@HsaFtH

The cytotoxicity of Diph@HsaFtH was assayed using Caco-2 and UKF-NB-4 cells. For this purpose, ~30,000 cells were seeded into 96-well plates and cultured for 24 h. After treatment with annotated concentrations of free Diph, empty HsaFtH, or Diph@HsaFtH, cells were incubated for 24 h, and viability was examined using the Cell Counting Kit-8 (Dojindo Molecular Technologies, Munich, Germany), according to the manufacturer's instructions. All experiments were performed in triplicate, with two independent runs.

Evaluation of Antiviral Activity

UKF-NB-4 (ZIKV, TBEV, and WNV) and Caco-2 (SARS-CoV-2) cells were cultured as previously described. After the formation of confluent monolayer (24 h), free Diph, empty HsaFtH and Diph@HsaFtH were added to a medium containing 0.1 MOI of ZIKV, WNV, or SARS-CoV-2. After 48 h of incubation, the medium containing viral particles was harvested and tested using a plaque assay to confirm the inhibitory effects of the treatment on the antiviral activity of the model viruses. Vehicle (DMSO) and empty HsaFtH were used as controls. All experiments were performed in triplicates in two independent experiments.

Plaque Assay

Plaque assays were performed using Vero cells in 24-well plates, in which the medium harvested from the antiviral activity assays, containing virus particles, was diluted 10-fold. Next, ~120,000 cells were added and the plates were incubated (3 h). After incubation, 3% carboxymethylcellulose mixed to culture medium (1:1, *v/v*) was added. After 5 days of incubation, the well plates were stained with naphthalene black according to Stefanik et al.[4] All experiments were performed in two independent experiments in triplicate.

Immunofluorescence of Viral Antigens

The antiviral activities of free Diph, empty HsaFtH, and Diph@HsaFtH were examined by fluorescence microscopy. Forty-eight-hour post-infection, the cells were fixed with a cold (−20 °C) acetone-methanol mixture (1:1, *v/v*). After that, cells were treated with 10% FBS to block the cellular surface proteins. To visualize viral antigen expression, *Flaviviridae* viruses (ZIKV and WNV in UKF-NB-4 cells) were stained using a mouse monoclonal antibody against the flavivirus group surface antigen (protein E) (1:250, antibody clone D1-4G2-4-15, Sigma-Aldrich). SARS-CoV-2 antigen expression in Caco-2 cells was assessed by staining with rabbit anti-spike S1 antibody (1:50, Sino Biological, Dusseldorf, Germany). Subsequently, the cells were incubated for 1 h at 37 °C, washed, and incubated with anti-rabbit goat secondary antibody conjugated with fluorescein isothiocyanate (FITC, 1:250) or anti-mouse goat secondary antibody conjugated with FITC (1:500). After incubation and washing, the nuclei were counterstained with 4′,6-diamidino-2-phenylindole (DAPI, 1 µg/mL). The fluorescence signal was recorded using an Olympus IX71 epifluorescence microscope and processed using ImageJ (National Institutes of Health, Bethesda, MA, USA).

Statistical Analysis

GraphPad Prism software was used for statistical analysis. The significance of cell viability in the Diph and Diph@HsaFtH groups and the significance of the comparison between the inhibitory activities of Diph and Diph@HsaFtH was calculated using two-way ANOVA. $*P < 0.05$; $**P < 0.01$; $***P < 0.001$; $****P < 0.0001$. The Shapiro–Wilk test was used to assess the normality of the analyzed data.

Results and Discussion

Formulation and Characterization of Diph@HsaFtH Nanoparticles

Although Diph acts as a potent V-ATPase inhibitor, its physicochemical properties affect its efficacy in vivo. To improve the disadvantageous properties of compounds with low bioavailability, various drug delivery systems have been successfully exploited.[23] Among them, various types of ferritins have been employed to enhance the bioavailability of poorly soluble compounds such as wogonin, vandetanib, lenvatinib, and others.[24,25] Therefore, in the present study, we employed recombinant HsaFtH to prepare a first Diph protein-based nanoformulation and subsequently test its biological properties with a special emphasis on antiviral activity against ZIKV, WNV, TBEV and SARS-CoV-2.

To load HsaFtH with Diph, an active encapsulation route based on pH-mediated reversible reassembly of HsaFtH subunits, followed by purification, was utilized (schematically depicted in Figure 1A). It should be noted that we also attempted to load HsaFtH using a passive route based on the diffusion of Diph into the internal cavity of HsaFtH through flexible channels (3–5 Å) between the subunits junctions.[26] However, the loading efficiencies were unsatisfactory, most

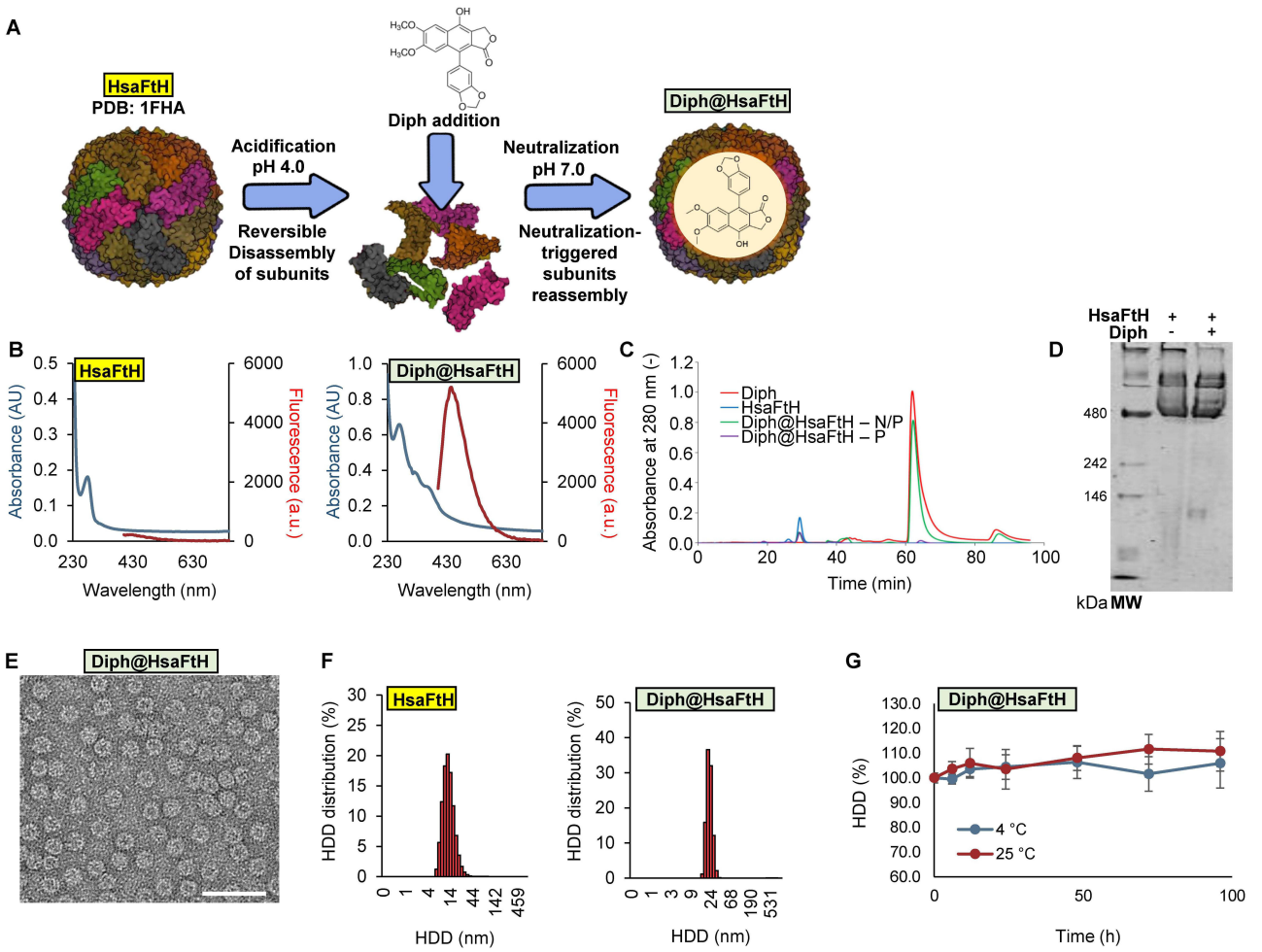

Figure 1 Formulation of Diph@HsaFtH and its physicochemical characterization. (**A**) Schematic depiction of a loading of Diph into the internal cavity of HsaFtH using active pH-mediated reversible reassembly of HsaFtH. (**B**) Absorption (blue line) and fluorescence (red line) spectra of HsaFtH (*left*) and Diph@HsaFtH (*right*). (**C**) FPLC-SEC chromatogram of free Diph, empty HsaFtH, non-purified (N/P) Diph@HsaFtH and purified (P) Diph@HsaFtH. (**D**) Native PAGE confirming successful reassembly of HsaFtH upon Diph loading. (**E**) TEM micrograph showing the morphology and homogeneity of Diph@HsaFtH nanoparticular dispersion. Scale bar, 50 nm. (**F**) HDDs of HsaFtH (*left*) and Diph@HsaFtH (*right*). Inserted are values describing PdI, surface ζ-potential and final concentration of encapsulated Diph. (**G**) Relative HDDs of Diph@HsaFtH incubated at 4 °C and 25 °C for up to 96 h showing a good stability of Diph@HsaFtH dispersion in water.

Abbreviations: Diph, diphyllin; HsaFtH, human *H*-ferritin; FPLC-SEC, fast protein liquid chromatography – size exclusion chromatography; PAGE, polyacrylamide gel electrophoresis; TEM, transmission electron microscopy; HDDs, hydrodynamic diameters; PdI, polydispersity index.

likely due to the low solubility/incompatible charge of Diph, which affected its diffusion into the HsaFtH cavity channel pores lined with negatively charged residues.[27]

After diafiltration, the Diph@HsaFtH nanoparticles were characterized by spectrofluorimetry and FPLC-SEC. As shown in Figure 1B, loading with Diph resulted in a hyperchromic shift of the absorption peak of HsaFtH (280 nm) and new absorption signals at slightly longer wavelengths (335 and 400 nm). Furthermore, after excitation with a λ_{exc} of 330 nm, the emission peak of Diph with a maximum of ~455 nm occurred, confirming the successful loading of Diph in HsaFtH. In addition, the FPLC-SEC chromatograms in Figure 1C demonstrate that multiple diafiltration steps removed the majority of unencapsulated Diph.

As shown by Kim et al, acidification of ferritin can induce hole effects[28] that can have deleterious effects on its quaternary structure. As demonstrated by native PAGE (Figure 1D), Diph@HsaFtH retained the original migration pattern of the empty non-reassembled HsaFtH. Furthermore, TEM revealed a highly homogeneous dispersion of hollow spherical nanocages without any observable structural defects or aggregation (Figure 1E). DLS confirmed that no significant HDD changes occurred due to Diph loading, while the loading slightly shifted ζ-potential (from −8.0 ± 0.4 mV for HsaFtH to −10.3 ± 0.7 mV for Diph@HsaFtH) (Figure 1F). Interestingly, the Diph@HsaFtH dispersion exhibited

Table 1 Physico-Chemical Properties of HsaFtH and Diph@HsaFtH

	PdI (-)	ζ-potential (mV)	c_{diph} (μg/mg of HsaFtH)
HsaFtH	0.455 ± 0.07	−8.0 ± 0.4	0.0
Diph@HsaFtH	0.366 ± 0.04	−10.3 ± 0.7	390.7 ± 26.3

a slightly better PdI, which was plausibly due to multiple diafiltration steps not performed with empty HsaFtH. UV-Vis spectrophotometry was used to determine that the final optimized formulation contains ~390.7 ± 26.3 μg of Diph per mg of HsaFtH (Table 1). Finally, a stability of Diph@HsaFtH dispersion in water was examined. Figure 1G shows that during the analyzed period (96 h), no significant increase in the relative HDDs was observed for both storage conditions; however, storage at 4 °C seems to perform better in particular for a longer-term storage. Taken together, HsaFtH proved to be a promising vehicle for facile and reproducible loading of sufficient amounts of Diph.

Evaluation of the Biocompatibility of Diph@HsaFtH in vitro

In the follow-up experiments, we aim to understand the properties of Diph@HsaFtH in biological systems in vitro. The natural ability of HsaFtH is to be internalized through TfR1 via receptor-mediated endocytosis,[29] followed by subsequent exposure to acidic pH and proteases within the endosomal lumen.[30] Since the sustained endosomal release is a crucial prerequisite for the functionality of the V-ATPase inhibitory activity of Diph loaded in HsaFtH, we first determined its release kinetics in buffers mimicking plasma (pH 7.4) and endosomal lumen (pH 5.0) environments (Figure 2A). We found that incubation of Diph@HsaFtH at acidic pH resulted in enhanced sustained release of Diph; at the experimental

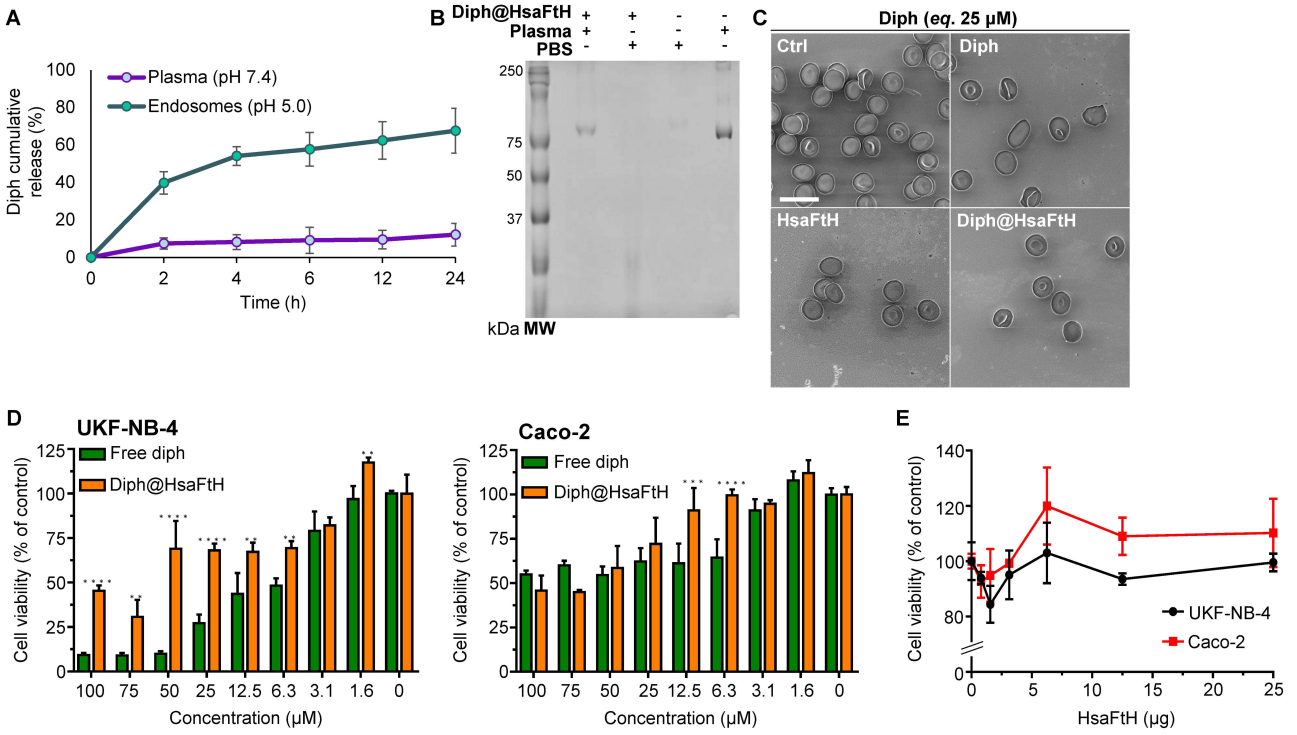

Figure 2 Evaluation of the biological properties of Diph@HsaFtH in vitro. (**A**) Cumulative release kinetics of Diph from Diph@HsaFtH incubated in plasma- or endosomal environment-mimicking buffers. (**B**) SDS-PAGE gel showing only a neglectable formation of plasma hard protein Corona of the surface of Diph@HsaFtH. The plasma lane shows plasma diluted 1000× with PBS. (**C**) SEM micrographs of human RBCs incubated with free HsaFtH, free Diph or Diph@HsaFtH. Scale bars, 10 μm. (**D**) Analysis of the cytotoxicity of free Diph and Diph@HsaFtH in UKF-NB-4 (*left*) and Caco-2 (*right*) cells. (**E**) Evaluation of the cytotoxicity of relevant concentrations of empty HsaFtH. Statistical analysis was carried out using Shapiro–Wilk normality test, and two-way ANOVA, $^{**}P < 0.01$; $^{***}P < 0.001$; $^{****}P < 0.0001$.

Abbreviations: Diph, diphyllin; HsaFtH, human *H*-ferritin; SDS-PAGE, sodium dodecyl sulfate-polyacrylamide gel electrophoresis; SEM, scanning electron microscopy; RBCs, red blood cells.

end-point (24 h), ~68% of Diph was released from the HsaFtH cavity with a Diph release half-life of ~4 h. In contrast, incubation in a plasma-mimicking environment resulted in only negligible Diph release (~12% of Diph at 24 h), suggesting that Diph@HsaFtH was sufficiently stable during the systemic circulation. These results are in line with the release kinetics of various drugs from ferritins,[12,16,25,31] underpinning the importance of endosomal environment-responsive release.

As the previous experiment demonstrated the exceptional circulation stability of Diph@HsaFtH, we next studied the interactions between Diph@HsaFtH and the blood circulation elements. During circulation, a range of plasma proteins can spontaneously adsorb onto the surface of a delivery vehicle to form a protein corona. The dynamic assembly of the protein corona can affect the recognition of nanomaterials by the innate immune system, phagocytic clearance, and ultimately the immunotoxicity of the delivery system.[32] Importantly, the protein corona can destabilize the nanoparticles and inhibit their ability to cross biological barriers.[33] The gel image in Figure 2B demonstrating only a minor amount of plasma proteins eluted from Diph@HsaFtH, confirming the intrinsic good blood stability of HsaFtH. Subsequent experiments with human RBCs have revealed that Diph may be hemotoxic. The SEM micrograph in Figure 2C shows obvious morphological changes in RBCs (anisocytosis and the presence of poikilocytes) after incubation with free Diph. Importantly, this response of RBCs was not observed after incubation with HsaFtH and Diph@HsaFtH, indicating that loading Diph into HsaFtH promotes protective effects against the undesired hemotoxicity of free Diph.

We then conducted a comparative study of the cytotoxicity of free Diph vs Diph@HsaFtH in UKF-NB-4 and Caco-2 cells, which are cellular models commonly used to study ZIKV, WNV, TBEV, and SARS-CoV-2 infections in vitro.[4,5] As shown in Figure 2D, in UKF-NB-4 cells, loading into HsaFtH markedly decreased the unwanted cytotoxicity of a wide range of Diph concentrations. This phenomenon was not as evident in Caco-2 cells, where a significant ($P < 0.001$; $P < 0.0001$) protective effect of HsaFtH loading was particularly observed for 12.5 and 6.3 μM Diph. This could be plausibly explained by the differential sensitivity of the two tested cell lines to Diph released upon the internalization of Diph@HsaFtH. To further rule out the potential contribution of HsaFtH to the cytotoxicity of Diph@HsaFtH, we analyzed the properties of the relevant amounts of empty HsaFtH. The empty delivery vehicle was found to be fully biocompatible in all samples tested, thus not synergizing with the cytotoxicity of Diph (Figure 2E). Therefore, HsaFtH acts as a smart pH-triggerable delivery system suitable for improving the undesired cytotoxic behavior of Diph.

Investigation of a Broad-Spectrum Antiviral Activity of Diph@HsaFtH

After assessing the biocompatibility of Diph@HsaFtH, we analyzed its antiviral activity. Several previously published studies have confirmed the broad-spectrum antiviral properties of Diph against various types of viruses.[4,5,10,11,34] In agreement with these studies, we confirmed that Diph acts as a potent antiviral compound capable of inhibiting ZIKV, WNV TBEV, and SARS-CoV-2 replication in vitro (Figure 3A). First, our analyses revealed that the empty HsaFtH did not exhibit antiviral activity (Figure 3B). After loading into HsaFtH, Diph retained its antiviral properties; however, loading into HsaFtH slightly decreased the antiviral potency of Diph. This phenomenon was further confirmed by spatial immunofluorescence analysis of ZIKV (Paraiba_01), WNV (13–104) and SARS-CoV-2 viral antigens, which also confirmed the slightly lower antiviral activity of Diph@HsaFtH than that of free Diph (Figure 3C). This can be explained by the substantially more complex mechanism required to release Diph from the Diph@HsaFtH. While free Diph can act immediately in a burst manner, Diph@HsaFtH requires the involvement of receptor-ligand interactions, followed by endocytosis, after which sustained release of Diph is triggered. This complicates the comparative antiviral analysis of free vs encapsulated Diph at the same time points. However, it can be expected that while the activity of Diph@HsaFtH could have a slower onset compared to free Diph, its antiviral activity could last longer and in a rather sustained manner, which is of general interest for real therapeutic scenarios.[35] It should also be noted that in Caco-2 cells, free Diph exhibited profound inherent cytotoxicity, observable as a dramatic decrease in host cell numbers (Figure 3A and C). This phenomenon was markedly alleviated by loading Diph into HsaFtH, highlighting its functionality as a delivery system.

It is worth noting that to the best of our knowledge, this is the first study to demonstrate the use of a recombinant protein-based delivery system to improve the properties of the V-ATPase inhibitor Diph. In addition to their exceptional biocompatibility, biodegradability, and the possibility of facile large-scale recombinant production of highly

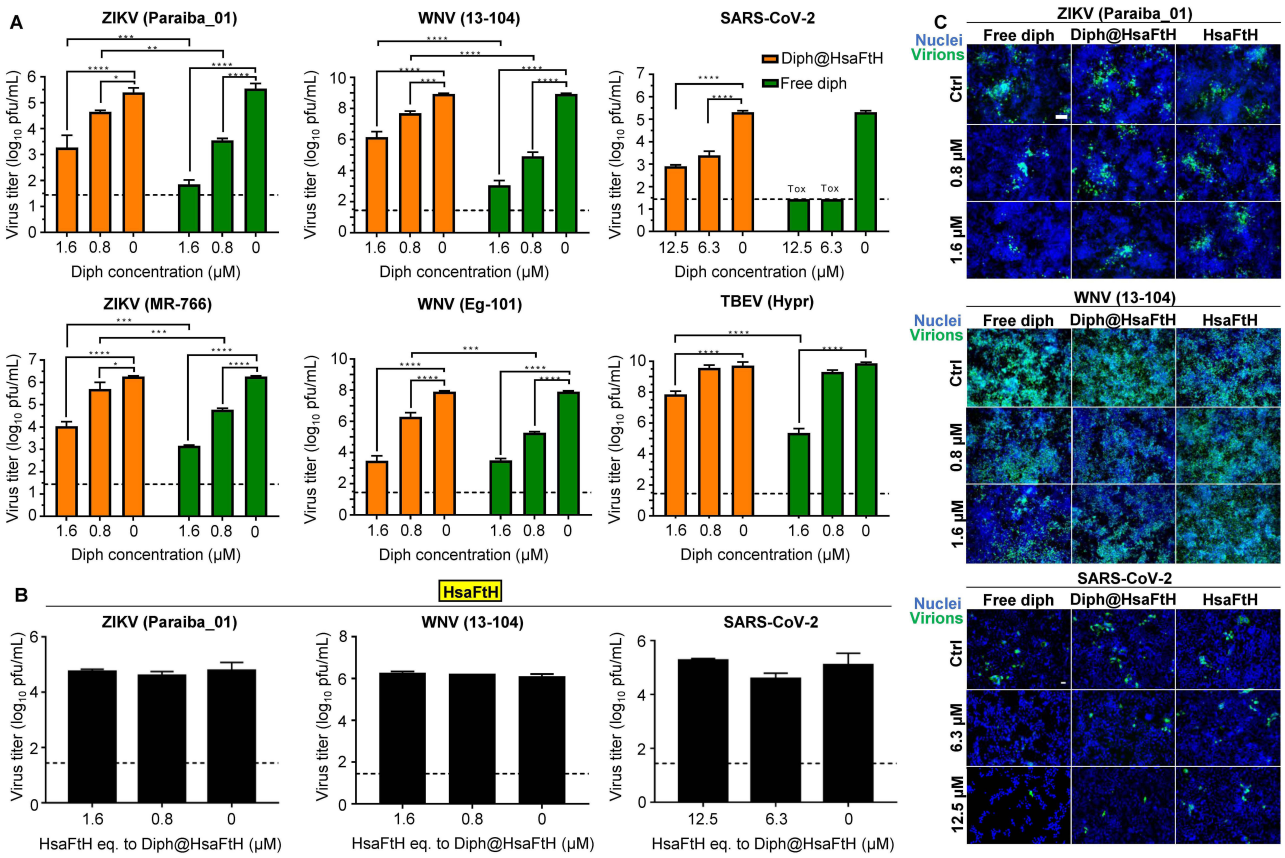

Figure 3 Assessing the antiviral properties of Diph@HsaFtH. Evaluation of inhibition of replication of ZIKV, WNV, TBEV and SARS-CoV-2 using (**A**) Diph@HsaFtH and (**B**) empty HsaFtH (amounts of empty HsaFtH are equal to the amounts of HsaFtH used in 12.5; 6.3 and 0 μM Diph@HsaFtH nanoformulations). (**C**) Immunofluorescence micrographs showing viral load (antibody-labelled viral antigens, *green*) in host cells (nuclei, *blue*). Scale bar, 80 μm. Statistical analysis was carried out using Shapiro–Wilk normality test, and two-way ANOVA, **P* < 0.05; ***P* < 0.01; ****P* < 0.001; *****P* < 0.0001.

Abbreviations: Diph, diphyllin; HsaFtH, human *H*-ferritin; ZIKV, Zika virus; WNV, West Nile virus; TBEV, tick-borne encephalitis virus; SARS-CoV-2, Severe acute respiratory syndrome-related coronavirus.

homogeneous nanoparticles, ferritins can be simply surface-modified to introduce small molecule/macromolecular targeting ligands to improve the selectivity of nanovehicles targeting diseased tissues.[36–38] This strategy could be adopted to promote the targeting of antiviral drugs, thus enhancing therapeutic outcomes. In this regard, we are eager to continue our work.

Conclusion

In this study, we demonstrated that the V-ATPase inhibitor Diph acts as a broad-spectrum antiviral compound. To improve the possible translational potential of Diph, which displays disadvantageous properties for preclinical studies, we exploited the recombinant HsaFtH and optimized a facile and efficient loading process capable of producing a highly homogeneous dispersion of stable nanoparticles with pH-responsive properties. In vitro analyses revealed that HsaFtH enhanced the safety of Diph in host cells. It was also found that upon loading, Diph exhibits a slightly lower antiviral activity compared to free Diph. This is possibly due to a more complex internalization/Diph release mechanism requiring HsaFtH-receptor interaction and receptor-mediated endocytosis that is not needed for freely diffusing non-encapsulated Diph. However, despite the lower antiviral activity of Diph@HsaFtH in vitro, it can be hypothesized that the nanoformulation will exhibit better properties in an in vivo scenario, in which HsaFtH can positively modulate Diph bioavailability and pharmacokinetics. This warrants further follow-up preclinical studies aimed on optimizing the Diph@HsaFtH dosing scheme (single dose vs repeated doses) and administration route (i.v. vs i.p.) to achieve the best possible therapeutic outcomes and a deeper understanding of Diph@HsaFtH as broad-spectrum antiviral nanoformulation.

Abbreviations

Diph, diphyllin; PEG-PLGA, poly(ethylene glycol)-block-poly(lactide-co-glycolide); HsaFtH, human *H*-ferritin; ZIKV, Zika virus; WNV, West Nile virus; TBEV, tick-borne encephalitis virus; SARS-CoV-2, Severe acute respiratory syndrome-related coronavirus; FLB, ferritin lysis buffer; TEM, transmission electron microscopy; DLS, dynamic light scattering; DMSO, dimethyl sulfoxide; HDD, hydrodynamic diameter; PdI, polydispersity index; SDS-PAGE, sodium dodecyl sulfate-polyacrylamide gel electrophoresis; FPLC-SEC, fast protein liquid chromatography – size exclusion chromatography; RBCs, red blood cells; SEM, scanning electron microscopy; MOI, multiplicity of infection; FBS, fetal bovine serum; FITC, fluorescein isothiocyanate; DAPI, 4′,6-diamidino-2-phenylindole.

Funding

Financial support was provided by the Internal Grant Agency of Mendel University in Brno (project no. AF-IGA2023-IP-025) and ERDF "Multidisciplinary research to increase the application potential of nanomaterials in agricultural practice" (No. CZ.02.1.01/0.0/0.0/16_025/0007314). This study was also supported by the National Institute of Virology and Bacteriology (Programme EXCELES, ID Project No. LX22N-PO5103) – Funded by the European Union – Next Generation EU. MV would like to express her gratitude to Brno Ph.D. Talent.

Disclosure

The authors report no conflicts of interest in this work.

References

1. Mathieu E, Ritchie H, Rodes-Guirao L, et al. Coronavirus Pandemic (COVID-19). OurWorldInData.org; 2020. Available from: https://ourworldindata.org/coronavirus. Accessed February 8, 2023.
2. De Clercq E, Li GD. Approved antiviral drugs over the past 50 years. *Clin Microbiol Rev*. 2016;29(3):695–747. doi:10.1128/CMR.00102-15
3. Chen R, Wang TT, Song J, et al. Antiviral drug delivery system for enhanced bioactivity, better metabolism and pharmacokinetic characteristics. *Int J Nanomed*. 2021;16:4959–4984. doi:10.2147/IJN.S315705
4. Stefanik M, Bhosale DS, Haviernik J, et al. Diphyllin shows a broad-spectrum antiviral activity against multiple medically important enveloped RNA and DNA viruses. *Viruses*. 2022;14(2):1–21. doi:10.3390/v14020354
5. Stefanik M, Strakova P, Haviernik J, Miller AD, Ruzek D, Eyer L. Antiviral activity of vacuolar ATPase blocker diphyllin against SARS-CoV-2. *Microorganisms*. 2021;9(3):1–10. doi:10.3390/microorganisms9030471
6. Sorensen MG, Henriksen K, Neutzsky-Wulff AV, Dziegiel MH, Karsdal MA. Diphyllin, a novel and naturally potent V-ATPase inhibitor, abrogates acidification of the osteoclastic resorption lacunae and bone resorption. *J Bone Miner Res*. 2007;22(10):1640–1648. doi:10.1359/jbmr.070613
7. Forgac M. Vacuolar ATPases: rotary proton pumps in physiology and pathophysiology. *Nat Rev Mol Cell Biol*. 2007;8(11):917–929. doi:10.1038/nrm2272
8. Staring J, Raaben M, Brummelkamp TR. Viral escape from endosomes and host detection at a glance. *J Cell Sci*. 2018;131(15):1–8. doi:10.1242/jcs.216259
9. Mitchell MJ, Billingsley MM, Haley RM, Wechsler ME, Peppas NA, Langer R. Engineering precision nanoparticles for drug delivery. *Nat Rev Drug Discov*. 2021;20(2):101–124. doi:10.1038/s41573-020-0090-8
10. Hu CMJ, Chen YT, Fang ZS, Chang WS, Chen HW. Antiviral efficacy of nanoparticulate vacuolar ATPase inhibitors against influenza virus infection. *Int J Nanomed*. 2018;13:8579–8593. doi:10.2147/IJN.S185806
11. Cmj H, Chang WS, Fang ZS, et al. Nanoparticulate vacuolar ATPase blocker exhibits potent host-targeted antiviral activity against feline coronavirus. *Sci Rep*. 2017;7(1):1–11. doi:10.1038/s41598-016-0028-x
12. Fan KL, Jia XH, Zhou M, et al. Ferritin nanocarrier traverses the blood brain barrier and kills glioma. *ACS Nano*. 2018;12(5):4105–4115. doi:10.1021/acsnano.7b06969
13. Operti MC, Bernhardt A, Grimm S, Engel A, Figdor CG, Tagit O. PLGA-based nanomedicines manufacturing: technologies overview and challenges in industrial scale-up. *Int J Pharm*. 2021;605:1–12. doi:10.1016/j.ijpharm.2021.120807
14. Tesarova B, Musilek K, Rex S, Heger Z. Taking advantage of cellular uptake of ferritin nanocages for targeted drug delivery. *J Control Release*. 2020;325:176–190. doi:10.1016/j.jconrel.2020.06.026
15. Heger Z, Skalickova S, Zitka O, Adam V, Kizek R. Apoferritin applications in nanomedicine. *Nanomedicine*. 2014;9(14):2233–2245. doi:10.2217/nnm.14.119
16. Kuruppu AI, Zhang L, Collins H, Turyanska L, Thomas NR, Bradshaw TD. An apoferritin-based drug delivery system for the tyrosine kinase inhibitor gefitinib. *Adv Healthc Mater*. 2015;4(18):2816–2821. doi:10.1002/adhm.201500389
17. Zhen ZP, Tang W, Chuang YJ, et al. Tumor vasculature targeted photodynamic therapy for enhanced delivery of nanoparticles. *ACS Nano*. 2014;8(6):6004–6013. doi:10.1021/nn501134q
18. Crich SG, Cadenazzi M, Lanzardo S, et al. Targeting ferritin receptors for the selective delivery of imaging and therapeutic agents to breast cancer cells. *Nanoscale*. 2015;7(15):6527–6533. doi:10.1039/C5NR00352K
19. He JY, Fan KL, Yan XY. Ferritin drug carrier (FDC) for tumor targeting therapy. *J Control Release*. 2019;311:288–300. doi:10.1016/j.jconrel.2019.09.002

20. Kidane TZ, Sauble E, Linder MC. Release of iron from ferritin requires lysosomal activity. *Am J Physiol Cell Physiol*. 2006;291(3):445–455. doi:10.1152/ajpcell.00505.2005
21. Sun CJ, Yuan Y, Xu ZH, et al. Fine-Tuned H-ferritin nanocage with multiple gold clusters as near-infrared kidney specific targeting nanoprobe. *Bioconjugate Chem*. 2015;26(2):193–196. doi:10.1021/bc5005284
22. Tesarova B, Dostalova S, Smidova V, et al. Surface-PASylation of ferritin to form stealth nanovehicles enhances in vivo therapeutic performance of encapsulated ellipticine. *Appl Mater Today*. 2020;18:1–11.
23. Parodi A, Buzaeva P, Nigovora D, et al. Nanomedicine for increasing the oral bioavailability of cancer treatments. *J Nanobiotechnol*. 2021;19(1):1–19. doi:10.1186/s12951-021-01100-2
24. Yang BY, Dong YX, Xu ZC, Li X, Wang F, Zhang Y. Improved stability and pharmacokinetics of wogonin through loading into PASylated ferritin. *Colloids Surf B*. 2022;216:1–9. doi:10.1016/j.colsurfb.2022.112515
25. Skubalova Z, Rex S, Sukupova M, et al. Passive diffusion vs active pH-dependent encapsulation of tyrosine kinase inhibitors vandetanib and lenvatinib into folate-targeted ferritin delivery system. *Int J Nanomed*. 2021;16:1–14. doi:10.2147/IJN.S275808
26. Tosha T, Behera RK, Ng HL, Bhattasali O, Alber T, Theil EC. Ferritin protein nanocage ion channels gating by N-terminal extensions. *J Biol Chem*. 2012;287(16):13016–13025. doi:10.1074/jbc.M111.332734
27. Takahashi T, Kuyucak S. Functional properties of threefold and fourfold channels in ferritin deduced from electrostatic calculations. *Biophys J*. 2003;84(4):2256–2263. doi:10.1016/S0006-3495(03)75031-0
28. Kim M, Rho Y, Jin KS, et al. pH-dependent structures of ferritin and apoferritin in solution: disassembly and reassembly. *Biomacromolecules*. 2011;12(5):1629–1640. doi:10.1021/bm200026v
29. Li L, Fang CJ, Ryan JC, et al. Binding and uptake of H-ferritin are mediated by human transferrin receptor-1. *Proc Natl Acad Sci U S A*. 2010;107(8):3505–3510. doi:10.1073/pnas.0913192107
30. Huotari J, Helenius A. Endosome maturation. *EMBO J*. 2011;30(17):3481–3500. doi:10.1038/emboj.2011.286
31. Liang M, Fan K, Zhou M, et al. H-ferritin-nanocaged doxorubicin nanoparticles specifically target and kill tumors with a single-dose injection. *Proc Natl Acad Sci U S A*. 2014;111(41):14900–14905. doi:10.1073/pnas.1407808111
32. Lee YK, Choi EJ, Webster TJ, Kim SH, Khang D. Effect of the protein Corona on nanoparticles for modulating cytotoxicity and immunotoxicity. *Int J Nanomed*. 2015;10:97–112.
33. Mahmoudi M, Landry MP, Moore A, Coreas R. The protein Corona from nanomedicine to environmental science. *Nat Rev Mater*. 2023;8(7):422–438. doi:10.1038/s41578-023-00552-2
34. Asano J, Chiba K, Tada M, Yoshii T. Antiviral activity of lignans and their glycosides from Justicia procumbens. *Phytochem*. 1996;42(3):713–717. doi:10.1016/0031-9422(96)00024-6
35. Delshadi R, Bahrami A, McClements DJ, Moore MD, Williams L. Development of nanoparticle-delivery systems for antiviral agents: a review. *J Control Release*. 2021;331:30–44. doi:10.1016/j.jconrel.2021.01.017
36. Zivotska H, Mokry M, Rodrigo MAM, et al. Conotoxin-derived biomimetic coiled cone-shaped peptide as ligand for selective nanodelivery to norepinephrine transporter-expressing neuroblastoma cells. *Appl Mater Today*. 2022;27:1–14.
37. Kaur N, Popli P, Tiwary N, Swami R. Small molecules as cancer targeting ligands: shifting the paradigm. *J Control Release*. 2023;355:417–433. doi:10.1016/j.jconrel.2023.01.032
38. Srinivasarao M, Low PS. Ligand-targeted drug delivery. *Chem Rev*. 2017;117(19):12133–12164. doi:10.1021/acs.chemrev.7b00013